

Novel optical and statistical methods reveal colloid–wall interactions inconsistent with DLVO and Lifshitz theories

Poul Martin Hansen, Jakob Kisbye Dreyer, Jesper Ferkinghoff-Borg, Lene Oddershede *

Niels Bohr Institute, Blegdamsvej 17, DK-2100 Copenhagen Ø, Denmark

Received 21 May 2004; accepted 26 January 2005

Available online 6 May 2005

Abstract

We present an experimental method based on video microscopy to perform nanometer scale position detection of a micrometer bead in the direction along the propagation of the detection light. Using the same bead for calibration and detection significantly improves the in depth resolution in comparison to video microscopy methods from literature. This method is used together with an optical trap to measure interaction potentials between a glass surface and colloids made of polystyrene or silica at different electrolyte concentrations. The results are confirmed by an independent method where the optical trap is used in connection with a quadrant photodiode. Also, we present a maximum likelihood analysis method which considerably improves the spatial resolution of interaction potentials by optimizing the underlying potential function to fit all observed position distributions. The measured interaction potentials agree well with DLVO theory for small electrolyte concentrations; however, for larger electrolyte concentrations the potentials differ qualitatively from both DLVO and Lifshitz theory.

© 2005 Elsevier Inc. All rights reserved.

Keywords: Interactions; Potentials; Optical tweezers; Video; Colloid; Surface; DLVO; Lifshitz; Maximum likelihood

1. Introduction

Optically trapped microspheres have proven successful as highly sensitive force-measuring transducers [1,2]. Typically, distances which the microspheres move within the trap are determined by single particle tracking routines [3] or by imaging the scattered light from the trapping laser or a second laser onto a quadrant photodiode [4]. The single particle tracking and quadrant photodiode detection schemes have mostly proven successful in terms of an accurate determination of forces and distances in the plane orthogonal to the direction of propagation of the trapping laser light where a resolution of 1/10 pixel is not unusual [5].

However, in some cases the position of a colloid in the direction parallel to the propagation of the trapping laser light is of interest, e.g., when measuring the interaction potential between a bead and a surface [6,7]. In the cases reported

in [6–8] the axial position determination has been done by using TIRM in conjunction with an optical trap. The use of TIRM constrains the geometry of the system; the bead must be close to the glass slide where the evanescent field enters the sample which is typically the surface opposite of the surface where the trapping laser light enters the sample. The further away from the coverslip where the laser enters the sample, the more severe the spherical aberrations of the optical trap [9–11].

By our video-based method, which utilizes only the CCD image of the bead, the z position can be determined with a resolution of 5 nm at any position within the sample and for beads of any size. In a setup including a trapping laser, the method also applies close to the surface of the sample where the laser trap suffers the least from spherical aberrations. The principle of our method is similar to that proposed by Crocker and Grier [5], but an important difference is that we calibrate using the probing bead and therefore the spread in the sizes of the beads in a typical sample does not influence the precision of the method. This is probably the reason why our resolution in the direction parallel to the propagat-

* Corresponding author. Fax: +45 35325425.

E-mail address: oddershede@nbi.dk (L. Oddershede).

ing laser light is 5 nm whereas the one stated in [5] (called “in-depth resolution”) is 150 nm. In [12] a related method is proposed with a resolution of 5–10 nm. Since with the video microscopy method the position of a reference object on the surface can be traced simultaneously, our method can be used in cases where drift is a problem. In comparison to the TIRM or quadrant photodiode-based detection schemes, our video method has the disadvantage of a slow sampling rate, limited by the repetition rate of the CCD camera. However, the advantages of the video-based method are that it can be used anywhere in the sample, it is possible to account for drift of the surface, the absolute distance to the surface is known at all times, its accuracy precedes that of previous video-based methods (in the direction parallel to the light path), and its implementation is very simple.

We use this method to measure the interaction between polystyrene or silica beads and a clean glass surface in solutions of various electrolyte concentrations. The glass–polystyrene interactions are also measured by an independent method using only the forward scattered light from the trapping laser light and a quadrant photodiode detector as described in [13]; this method gives similar results. The measurements from both the video microscopy method and the quadrant photodiode method are significantly improved by a maximum-likelihood statistical analysis [14], which is hereby for the first time applied to this type of data. At low electrolyte concentrations our results reproduce those of DLVO theory; however, at larger electrolyte concentrations we see an interaction profile which is qualitatively different from existing theories.

We start by introducing some theoretical framework concerning surface–colloid interactions, and then the general principle we use for probing the surface. The two experimental methods invoked, the video microscopy and the quadrant photodiode based, are described. Then the maximum likelihood analysis of the measurements is described and finally, the results are presented and compared to existing theories.

2. Interactions between charged surfaces

The interactions between two surfaces immersed in a liquid comprise various forces of different origin. At separations larger than ~ 50 nm, the interactions are predominantly electrostatic while at smaller separations van der Waals attractions may become important too. These two types of interactions are combined in the DLVO theory. For low surface potentials, $|\psi| \leq 25$ mV, the electrostatic and van der Waals interactions between a sphere and an infinite flat surface separated at a distance z , can be approximated by [15]

$$\phi(z) = \phi_0 e^{-\kappa z} - U. \quad (1)$$

Here, κ^{-1} determines the length scale of the electrostatic interaction and is known as the Debye length. The constant ϕ_0 is given by $\phi_0 = 4\pi \epsilon_w \epsilon_0 \psi_{\text{glass}} \psi_{\text{bead}} R$, where R denotes the radius of the bead, ϵ_w is the permittivity of water, ϵ_0 is

the vacuum permittivity, and ψ_{bead} and ψ_{glass} denote the surface potentials of the bead and the glass surface, respectively. U is a measure of the van der Waals interaction and can be given by at least two different expressions of which one is the Derjaguin’s approximation [16],

$$U_D = \frac{AR}{6z}, \quad (2)$$

which is valid when $z \ll R$. However, U can also be given by a more exact result of the van der Waals interaction between a sphere and a surface which is also valid when $z \sim R$ through the surface element integration method (SEI) [17]:

$$U_{\text{SEI}} = \frac{A}{6} \left[\frac{R}{z} + \frac{R}{z+2R} + \ln \left(\frac{z}{z+2R} \right) \right]. \quad (3)$$

A is the Hamaker constant and depends on the materials of the interacting bodies. The repulsive interaction between the surfaces is highly dependent upon the electrolyte concentration in the surrounding fluid through the parameter κ :

$$\kappa = \sqrt{\frac{e^2 \sum_i \rho_i v_i^2}{\epsilon_w \epsilon_0 k_B T}} \text{ m}^{-1}. \quad (4)$$

Here, ρ_i is the density of the i th ion and v_i is the corresponding valency. Inserting the relevant parameters for an 1:1 electrolyte like NaCl yield a convenient expression for the Debye length,

$$\kappa^{-1} = \frac{0.304}{\sqrt{[\text{NaCl}]}} \text{ nm}, \quad (5)$$

where [NaCl] refers to the electrolyte concentration in moles per liter. The van der Waals interaction originates from the interaction between microscopic fluctuating dipoles which in the DLVO theory are integrated to yield the total attraction.

Two additional phenomena are included in the more comprehensive Lifshitz theory [18,19]: (1) The attraction falls off with separation distance due to decorrelation of the interacting dipoles. (2) The interactions are affected by screening from the free counterions between the two surfaces. According to the Lifshitz theory the functional form for the van der Waals interaction ϕ_{s-s} between two flat surfaces (s) is

$$\phi_{s-s}(z) = -\frac{A(z)}{12\pi z^2}. \quad (6)$$

Here, A is the Hamaker constant and z is the separation distance. The retardation and screening effects enter through the Hamaker constant which is a decaying function of z . The Hamaker constant depends on the material properties through the dielectric functions of the interacting plates and the medium separating the two surfaces. Complete dielectric functions for most materials are not determined, but for polystyrene and glass we used the parameters reported in [20].

3. Principle of surface probing

To measure interaction potentials between a glass surface and an optically trapped bead, time series of the position of the bead were recorded at different distances between the center of the trap and the surface. Typically, this distance was decreased in steps of 50 nm between each time series, the steps being sufficiently small to obtain substantial overlap in the positions of the bead between consecutive time series.

The force F exerted by the optical trap on a bead at position z is to a good approximation harmonic:

$$F(z) = -\kappa_t(z - z_0), \quad (7)$$

where κ_t is the stiffness of the optical trap and z_0 is the equilibrium position of the optical trap which in the absence of external forces equals the mean position of the trapped bead. The distribution of the bead positions is Gaussian. Under the influence of an external force, F_{ext} , this distribution will be shifted. At the new equilibrium position of the bead, z_b , the force exerted on the bead by the optical trap is equal in size but opposite to the force exerted by the surface interaction on the bead:

$$F_{\text{ext}}(z_b) = \kappa_t(z_b - z_0). \quad (8)$$

This relation allows for a determination of the external force acting on the bead by monitoring the shift in the position of the peak of the histogram.

Fig. 1 shows a series of histograms obtained from a number of time series of an optically trapped silica bead. Between each histogram the trap position, z_0 , was moved toward the glass surface in 50-nm steps. Far from the surface, where the interaction is negligible, the histograms are well fitted by a Gaussian function yielding κ_t and z_0 . As the interacting surface approaches the trapped bead, the peak of the histograms is shifted and the width of the histograms decreases due to the presence of external forces.

With this method all information obtained in each time series is utilized to produce one data point, giving the external force acting on the bead in the position z_b . However, in order to use the information stored in the time series more efficiently, we also used Boltzmann statistics to invert the

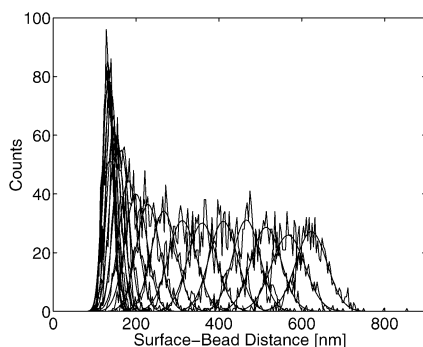


Fig. 1. Histograms showing the position of the trapped bead as the optical trap is moved in steps of 50 nm toward the surface. The abscissa is in relative, not absolute, units.

histograms into potential energy as explained in detail in Section 5.

4. Materials and methods

4.1. Video microscopy method

In the video microscopy method we basically utilize the fact that in bright-field microscopy the diffraction pattern from a bead changes as the bead moves from below to above the focus. Below the focus, the outer radius of the diffraction rings increase. Conversely, above the focus the diffraction rings become smaller and converge into a bright spot.

Two such diffraction patterns are shown in Fig. 2. The bead to the left is stuck to the surface and is below the focus of the microscope, whereas the bead to the right is held above by the optical trap in a position nearly coinciding with the focus of the microscope. In order to get a measure of how this diffraction pattern changes with the axial position of the bead with respect to the focus of the microscope objective we calculate the second moment of this brightness distribution [5]:

$$M_2 = \frac{1}{M_0} \sum_{ij, i^2+j^2 < r_0^2} (i^2 + j^2) I(x+i, y+j). \quad (9)$$

Here, r_0 is chosen to be approximately the maximum radius of the diffraction pattern. $M_0 = \sum_{ij, i^2+j^2 < r_0^2} I(x+i, y+j)$ is the integrated intensity inside an area of radius r_0 and $I(x, y)$ is the intensity of the pixel positioned at (x, y) . The unit of M_2 is pixels².

4.1.1. Calibration

A bead stuck to the surface is moved in a controlled fashion through the focus of the microscope objective. M_2 is calculated at each position of the surface. Consequently, a relationship between M_2 and the axial position of the bead can be obtained. From averaging a number of such runs a calibration curve shown as a full line in Fig. 3 is obtained. All parts of the calibration curve which have a one-to-one relation between M_2 and the axial position can in principle be used for position determination. However, for practical reasons we use the approximately linear region only. The dashed line in Fig. 3 is a linear fit to the region between the two horizontal lines. This fit gives a constant C_{video} which relates M_2 to the



Fig. 2. Microscope picture containing both a bead stuck to the surface (left) and a bead (right) in the optical trap the position of which nearly coincides with the focus of the microscope above the surface.

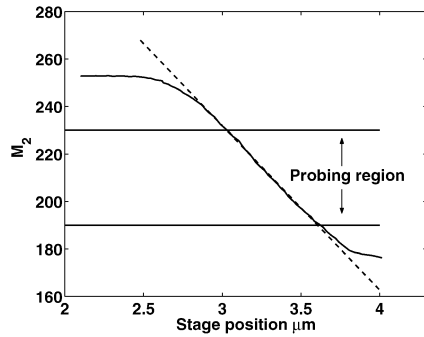


Fig. 3. M_2 as a function of position of the bead as the bead is moved through the focus of the microscope objective. The offset on the two axes is arbitrary. The dashed line is a linear fit to the part of the calibration curve between the two horizontal lines.

axial position of the bead, z_{rel} : $M_2 = C_{\text{video}} z_{\text{rel}}$. The characteristic size of the Brownian motion of a bead in the trap is significantly smaller than the linear region of the calibration curve. This method can be used to probe bead–surface interactions, even at large distances between bead and surface.

To keep track of the center pixel between successive frames we used a centroid tracking algorithm:

$$\begin{pmatrix} c_x \\ c_y \end{pmatrix} = \frac{1}{M_0} \sum_{i,j < |r_0|} \binom{i}{j} [I(x+i, y+j) - bg]. \quad (10)$$

The algorithm calculates a new center pixel only if the new center deviates more than 0.5 pixel in the x or y direction from the previous center and is similar to the algorithm used in [5]. A mask of size $2r_0 \times 2r_0$ including the bead was used to calculate the centroid center. To avoid any bias toward an artificial center the background intensity (bg) was subtracted and the centroid was calculated from the absolute value of the resulting intensity distribution [5].

The magnification on the CCD camera is 50 nm/pixel which corresponds to approximately $3 \times$ the standard deviation of a trapped bead in the focal plane. Therefore, the tracking algorithm typically assigns the same center pixel for the trapped bead. More importantly, it accounts for surface drift and crosstalk among the x , y , and z directions. To avoid artifacts an intensity threshold is used to skip unphysical values of the centroid procedure.

4.1.2. Procedure

The axial trap stiffness is determined from the width of position histograms as shown in Fig. 1 sufficiently far away to ignore proximity effects. The relation between the standard deviation of a Gaussian histogram, σ , and the trap stiffness, κ_t , is $\sigma^2 = k_B T / \kappa_t$.

In order to probe the interaction between the trapped bead and the surface of the perfusion chamber, the microscope objective and hence the optical trap is moved until the distance between the coverslip and bead is around 1 μm . Preferably, in the field of view of the microscope there should be two beads, one in the laser trap and the other stuck to the surface. The stuck bead is used as a reference, the motion of

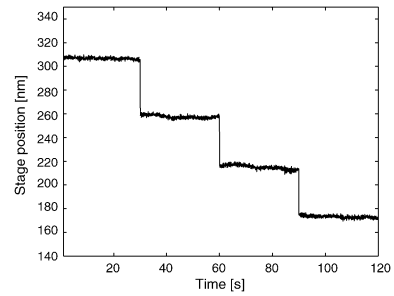


Fig. 4. Video method determinations of the position of a bead stuck to a surface which is moved in discrete steps of 50 nm. At each step, the typical level of noise and drift is visible.

which is subtracted from the measured motion in order to eliminate possible drift of the sample. Then, the surface is moved by the piezoelectric stage in steps of 50 nm toward the trapped bead. At each step, the fluctuations of the bead in the trap are recorded for 30 s by the CCD camera.

After completing the probing procedure, the bead is attached to the surface to perform the calibration. Since the size of the beads varies with about 10% it is crucial to perform the calibration for the same bead as the one used in the probing procedure. At moderate to high electrolyte concentrations it is possible to attach the bead by forcing it to the surface with the optical trap. At low electrolyte concentrations, however, this was not possible. In order to calibrate at low electrolyte concentrations, more electrolyte was added to the chamber to enable attachment of the bead the surface after the probing had ended. In all cases, the calibration curve is obtained by oscillating the stuck bead for 30 s with an amplitude of 1.6 μm and a period of 10 s.

4.1.3. Resolution and noise

In order to test the resolution of the method the diffraction pattern of a bead stuck to a surface was recorded as the stage was moved in discrete steps as shown in Fig. 4. At each step, the standard deviation of the noise was approximately 5 nm which we define as the resolution of our method. In Fig. 4 the drift of a stuck bead, that is, the drift of the glass coverslip is also visible. This drift is caused by various environmental disturbances such as temperature changes, mechanical vibrations, liquid evaporating, etc. While performing the measurements we eliminate the effect of this drift by subtracting the position of a stuck bead from the position of the probing bead.

There are a number of contributions to the noise of the signal: First, a readout noise is introduced in transforming the analog image from the CCD camera to digital form in the computer, increasing approximately as the square root of the readout rate. Readout noise is minimized by electrical shielding of the equipment and by using a CCD camera with a low readout frequency. Secondly, thermally excited photons in the CCD device contribute to a dark current. The gain is set to minimum thus suppressing any dark current. As the temperature inside the CCD camera exceeds the ambient laboratory temperature this can be a significant contribution

to the noise. Furthermore, static noise is added from geometrical distortions and dirt on the optics which we have tried to minimize. Finally, shot noise is always present in photon-counting measurements as it is intrinsic to the photon statistics. It can be reduced by increasing the exposure time of the camera but as this introduces correlation between the frames it is not a good solution. During experiments all the surrounding light was switched off to minimize stray light from entering the CCD camera.

4.2. Quadrant photodiode method

When a bead is trapped by the optical tweezers the total intensity of the forward scattered light carries information on the position of the trapped bead in the direction parallel to the propagation of the trapping laser light [21,22]. Within a few hundred nanometers around the focal point the intensity of the forward scattered light is proportional to the position of the bead. By measuring this intensity with a photodiode, sampling rates at mega Hertz and nanometer spatial resolution can be obtained.

4.2.1. Procedure

We calibrate the trap by analyzing the power spectrum of the positions of an optically trapped bead using the methods described in [24]. From the calibration we obtain the trap stiffness, κ_t , and a conversion factor, C_{qpd} , which relates the light intensity detected by the photodiode to the spatial coordinates of the trapped bead. Since it was found that the value of C_{qpd} changes as the trap position is moved toward the surface it is important to calibrate as close to the coverslip as possible, but still sufficiently far away to neglect surface interactions. In the measurements presented here the optical tweezers have been calibrated at a distance of $\simeq 400$ nm from the surface. This procedure is rather different from the calibration of the trap stiffness in the video microscopy-based method (see Section 4.1) where the distance to the coverslip typically is around 4 μm . As the distance between the surface and the bead is very small, the proximity of the surface substantially reduces the axial diffusion constant of the bead [25]; an effect which must be taken into account in the calibration procedure. We found that the trap stiffness, κ_t , was constant for bead-surface separations at least up to 700 nm. A small change in the offset of the photodiode intensity was found when the optical trap was closer than 700 nm to the surface; this is taken into account in the analysis of the data.

As previously shown [13], the sensitivity and the linear range of the position detection method can be controlled by a careful setting of the numerical aperture of the condenser, NA_{cond} . The desired sensitivity is achieved only in a narrow range of NA_{cond} , from 0.8 to 0.9. When NA_{cond} falls outside this region we observe periodic artifacts in the intensity signal, a phenomenon caused by multiple reflections of the trapping laser by the bead and the nearby surface [26].

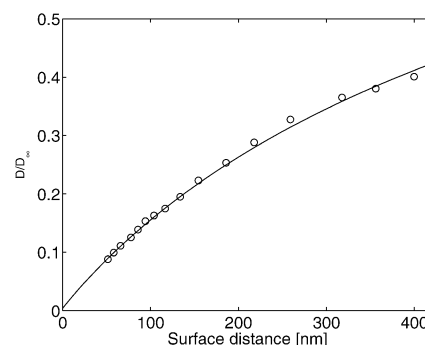


Fig. 5. Normalized diffusion constant as a function of distance to surface for a 1.07 μm polystyrene bead in 0.5 mM NaCl. The data points are based on time series recorded with the QPD. $\kappa_t = 0.003$ pN/nm. The solid line is a fit to the profile suggested by Brenner [25]. The distance from the bead to the surface and D_∞ are the free parameters in the fit.

A typical time series consists of 32768 data points, sampled at a rate of 4 kHz (anti-alias filtered at 2 kHz). After recording a time series, the distance between bead and surface is reduced by 30 nm by moving the piezo stage. We discard data recorded within 1 s after moving the piezo to eliminate transient effects.

4.2.2. Determination of absolute distance to coverslip

In the experiments conducted with the video methods, the position of a reference bead stuck on the surface can be obtained simultaneously with the position of the bead in the trap and hence the exact distance to the surface is known at all times. By the quadrant photodiode method, we cannot measure this directly. Instead, we determine the diffusion constant in each time series [24] and compare it to the theoretically expected diffusion profile which is distance dependent close to a surface [6,25]. Since our time resolution is much higher than the autocorrelation time it is possible to find the diffusion constant from a power spectral analysis [24]. Fig. 5 shows the normalized local diffusion constant, D/D_∞ , as a function of distance to the surface. D_∞ is the diffusion constant found by Stokes law in the limit far from the surface. We estimate the accuracy of this method to be around 30 nm from those rare time series where the bead actually got stuck to the surface at some point during the measurement.

4.3. Focus shift

Spherical aberrations stemming from a mismatch in the refractive indices of the glass and water at the interface in the microscope sample shift the position of the focal point. At positions far from the surface the relation between the position of the physical focus of the objective and the nominal focus is approximately linear: When the glass–water interface is moved Δz , the actual focus moves $FS\Delta z$ in the same direction, with FS being the constant of proportionality between the apparent focus and the actual focus. A similar concept holds for the positions of a trapped bead: Shifting the

surface by an amount Δz toward a trapped bead, the spherical aberrations will cause the distance between the trapped bead and the surface to be reduced only by

$$\Delta z_{\text{focus}} = (1 - FS)\Delta z. \quad (11)$$

Numerical calculations have determined FS to be around 0.3 [9,10]. These numbers are, however, rather different from our direct experimental measurements: By moving a stuck polystyrene bead in a controlled manner through the focus of the laser beam, the response of the intensity of the forward scattered light can be used for the measurement of FS . In this case, the change in scattering intensity, ΔV , is related to the change in bead position relative to the focal plane of the objective, ΔZ_{focus} . On the other hand, the conversion factor C_{qpd} , defined in Section 4.2.1, is also a measure of the magnitude of the change in scattering intensity upon movements of the bead. This conversion factor is obtained using the thermal fluctuations of the bead and does not involve FS . Therefore,

$$C_{\text{qpd}} = (1 - FS) \frac{\Delta Z}{\Delta V}, \quad (12)$$

which can be used to measure FS . Using this method for a bead close to the surface we found $FS \sim 0$ for polystyrene beads. To obtain physically acceptable interaction profiles with a 1-1 relation between separation distance and potential, our measurements confirm that the value $FS = 0$ is appropriate even at bead-surface distances up to 400 nm. The reason for the discrepancy between our results and that of [9,10] could be that the values for FS given in [9,10] are for systems where the absolute distance to the surface is larger than in our measurements, while in our experiment, the distance of interest is below 20% of the wavelength, rendering geometrical optics type of arguments inadequate.

Silica beads have different optical properties and are more heavy than the polystyrene beads. A similar measurement shows that $FS \sim 0.2$ for silica beads at distances close to the interface.

Altogether, the issue of how to treat spherical aberrations near the interface still remains to be settled and is an obvious subject for further investigations.

4.4. Equipment

The optical trap is based on a NdYVO₄ laser with wavelength 1064 nm and is implemented in an inverted microscope with a quadrant photodiode detection scheme [13,23]. The setup is shown in Fig. 6. A laser power of 10–20 mW, measured at the position of the sample, was used in all experiments. Data were acquired using a National Instruments card (PCI-MIO-16E-4). The sample was mounted on a three-axis translational piezoelectric stage (PI 731.20, Physik Instrumente, Germany) with capacitive feedback control and nanometer position resolution. The CCD camera is a Sony XC-EI50 with a repetition rate of 25 Hz. The CCD camera produces frames which are composed of two interlaced

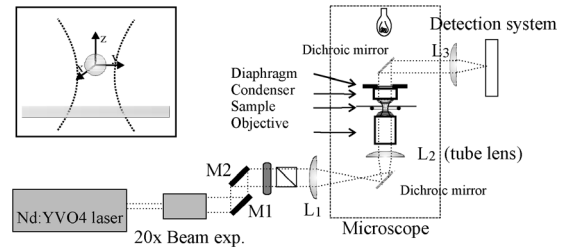


Fig. 6. Schematic of the setup. The quadrant photodiode is placed at the position of “Detection system.” The video camera is hooked up to the microscope objective.

fields consisting of the even and the odd pixel rows, respectively. To avoid mixing the positions represented by the even and the odd fields, respectively, only one of the fields were used to find the position of the bead. To minimize correlation artifacts the exposure time of the camera was set to $\tau = 2$ ms. The power of the illuminating lamp was adjusted such that the intensity distribution approximately filled the 8 bit dynamical range of the frame grabber. The temperature was fairly constant at 295 ± 2 K.

4.5. Sample preparation

The silica colloids (with diameter $d = 0.97 \mu\text{m}$, $\Delta d = \pm 10\%$) and polystyrene ($d = 1.07 \mu\text{m}$, $\Delta d = \pm 10\%$) were purchased from Bangs Laboratory Inc. The microspheres were washed in Millipore water and ultrasonicated to break agglomerates. The beads in solution were flushed into a perfusion chamber, the sides of which were thoroughly cleaned by ultrasonication in 96% ethanol. The sides of the chamber were separated by vacuum grease.

5. Maximum likelihood method

In this section it is explained how we utilize the data obtained by the video microscopy and quadrant photodiode methods to find the underlying potential of the interaction. More precisely, we derive a maximum-likelihood estimate, $\hat{\phi}(z)$, for the surface potential, $\phi(z)$, by combining the information of all histograms obtained at different trap-surface distances.

5.1. Most probable surface potential

Let $V_{z_0}(z)$ be the potential (in units of $k_B T$) associated with the force exerted by the optical trap centered at z_0 on a bead at position z , Eq. (7), i.e., $V_{z_0}(z) = \kappa_t(z - z_0)^2/2k_B T$. The probability, $\mathcal{P}_{z_0}(I(\bar{z})|\phi)$, for observing the bead within the interval $I(\bar{z}) = [\bar{z} - \Delta z/2, \bar{z} + \Delta z/2]$, given the external surface potential ϕ , will be

$$\mathcal{P}_{z_0}(z \in I(\bar{z})|\phi) = \frac{\int_{\bar{z}-\Delta z/2}^{\bar{z}+\Delta z/2} \exp(-V_{z_0}(z) - \phi(z)) dz}{\int \exp(-V_{z_0}(z) - \phi(z)) dz}.$$

Here, $\phi(z)$ is defined in units of $k_B T$ as well. By choosing a regular and sufficiently small bin width Δz , we obtain $\mathcal{P}_{z_0}(z \in I(\bar{z})|\phi) \approx p_{z_0}(\bar{z}|\phi)$, where

$$p_{z_0}(\bar{z}|\phi) = \frac{\exp(-V_{z_0}(\bar{z}) - \phi(\bar{z}))}{Z_{z_0}(\phi)}. \quad (13)$$

In this expression, $Z_{z_0}(\phi)$ is the partition function obtained by summing the Boltzmann weights over the discrete set of z values given by the midpoints of the bins,

$$Z_{z_0}(\phi) = \sum_z \exp(-V_{z_0}(z) - \phi(z)).$$

For an uncorrelated time series of bead positions, $\{z_t\}$, the accumulated histogram, $N(z)$, will be a member of the multinomial [27] probability distribution $P_{z_0}(N|\phi)$,

$$P_{z_0}(N|\phi) = n! \prod_z \frac{p_{z_0}(z|\phi)^{N(z)}}{N(z)!},$$

where $n = \sum_z N(z)$ is the total number of counts.

For a series of measurements $i = 1, \dots, M$ with different trap positions $(z_0)_i$, each histogram, $N_i(z)$, can be regarded as an observation of the corresponding multinomial distribution $P_i(N_i|\phi)$. Due to the mutual independence of the measurements the likelihood, $L(\vec{N}|\phi)$, of observing the full set $\vec{N} = (N_1, \dots, N_M)$ is simply given by a product of the P_i 's,

$$L(\vec{N}|\phi) = \prod_{i=1}^M P_i(N_i|\phi). \quad (14)$$

Our objective is to find the maximum-likelihood (ML) potential, $\hat{\phi}$, given the observations \vec{N} ; i.e., we wish to maximize $L(\phi|\vec{N})$ with respect to the function ϕ . From Bayes theorem [27] we have

$$L(\phi|\vec{N}) = \frac{L(\vec{N}|\phi)L(\phi)}{L(\vec{N})}, \quad (15)$$

where $L(\phi)$ and $L(\vec{N})$ are a priori probability distributions for the potential and the observations, respectively. Here, $L(\vec{N})$ only enters as a normalization constant and can therefore be discarded. In the following, we will assume no prior knowledge of the potential by setting $L(\phi) = \text{const}$. Consequently, $L(\phi|\vec{N}) \propto L(\vec{N}|\phi)$, so maximizing Eq. (14) with respect to ϕ will yield the desired estimate for the surface potential. Equating $\partial_{\phi(z)} \log L(\vec{N}|\phi) = 0$ gives

$$\exp(-\hat{\phi}(z)) = \frac{\sum_{i=1}^M N_i(z)}{\sum_{i=1}^M n_i Z_i(\phi)^{-1} \exp(-V_i(z))}, \quad (16)$$

where $n_i = \sum_z N_i(z)$. The partition functions Z_i must be estimated self consistently from Eq. (16). Expressed in terms of the unitless free energies, $f_i = -\log(Z_i)$, the partition functions can be found by solving the M equations, $j = 1, \dots, M$,

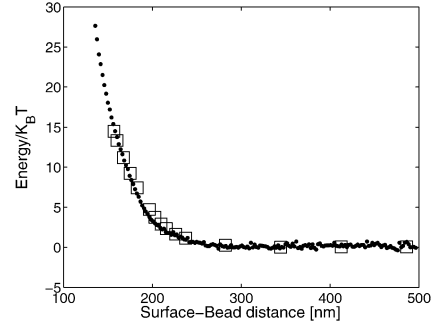


Fig. 7. The estimated interaction potential between a polystyrene bead and a glass surface in $[\text{NaCl}] = 0.1 \text{ mM}$ using video microscopy. The square symbols (\square) are the result from a numerical integration of the measured surface force according to Eq. (8). The dotted curve (\bullet) is the potential obtained by applying the maximum-likelihood method to the same data set. The method increases the spatial resolution by roughly one order of magnitude.

$$F_j(\vec{f}) \hat{=} \sum_z \frac{\sum_{i=1}^M N_i(z)}{\sum_{i=1}^M n_i \exp(V_j(z) - V_i(z) + f_i - f_j)} = 1, \quad (17)$$

where $\vec{f} = (f_1, \dots, f_M)$. Equations (16) and (17) are reformulations of the generalized multihistogram which were derived in the context of Monte Carlo sampling in [14]. Since an arbitrary constant can be added to all f_i without affecting the solution, the estimated surface potential, $\hat{\phi}$, is determined up to an additive constant only. This zero mode is easily removed by choosing a reference value, for instance $\phi(\infty) = 0$.

A convenient and fast approach for calculating $\hat{\phi}$ is first to find the solution to Eq. (17) using the globally convergent Newton–Rapson scheme [28] with the explicit expression for the Hessian, $H_{jk} = \partial F_j / \partial f_k$,

$$H_{jk} = \delta_{jk} F_j - n_k \exp(f_j + f_k) \times \left[\sum_z \frac{\sum_{i=1}^M N_i(z)}{(\sum_i n_i \exp(f_i - V_i(z)))^2} \right]. \quad (18)$$

Note that $H_{jk} = H_{kj} n_k / n_j$, so only $M(M + 1)/2$ elements of the Hessian need to be calculated. The change of variables, $Z_i \rightarrow f_i$ in Eqs. (17) and (18) is necessary to ensure numerical stability of the Newton–Rapson algorithm. From the solution, \hat{f} , to Eq. (17) one obtains the most probable potential, simply by substituting $Z_i = \exp(-\hat{f}_i)$ into Eq. (16).

In Fig. 7 we illustrate the power of the maximum-likelihood method as outlined in this section. The square symbols represent the surface energy obtained from a numerical integration of Eq. (8) using the procedure outlined in Section 3 for a polystyrene bead in $[\text{NaCl}] = 0.1 \text{ mM}$. Solving Eqs. (16) and (17) for the same data yields the energy profile represented by the dot symbols. By this procedure, the spatial resolution is improved by roughly one order of magnitude.

5.2. Effect of positional uncertainties of the optical trap

The derivation outlined above is based on the assumption that the distance, $(z_0)_i$, between the surface and the center of the trap is kept constant during the recording of each of the histograms N_i . In practice, $(z_0)_i$ will be subject to small fluctuations, drift, etc. It is important to analyze under which conditions these uncertainties can be neglected. The simplest way of accounting for them is to convolve the probabilities in Eq. (13) with an a priori probability, $P_{T_i}(z_0)$, for the trap to attain the center value z_0 at some instance during measurement i . The probability, $\tilde{p}_i(z)$, of observing the position z of the bead during measurement i will then be given by

$$\tilde{p}_i(z|\phi) = \exp(-\phi(z)) \left\langle \frac{\exp(-V_{z_0}(z))}{Z_{z_0}(\phi)} \right\rangle_{T_i}, \quad (19)$$

where $\langle q \rangle_{T_i} \hat{=} \sum_{z_0} P_{T_i}(z_0) q(z_0)$ for a z_0 -dependent quantity q . Let $(\bar{z}_0)_i$ be the most probable trap position in measurement i , and replace the z_0 -dependent term in Eq. (19) with $g(z, z_0)$ for notational convenience; $g(z, z_0) = \exp(-V_{z_0}(z))/Z_{z_0}(\phi)$. Assuming P_{T_i} to be symmetric around $(\bar{z}_0)_i$ we get from a Taylor expansion

$$\langle g \rangle_{T_i}(z) = g(z, (\bar{z}_0)_i) + \frac{1}{2} \frac{\partial^2 g(z, z_0)}{\partial z_0^2} \Big|_{(\bar{z}_0)_i} \sigma_{T_i}^2 + \dots,$$

where $\sigma_{T_i}^2 = \langle (z_0 - (\bar{z}_0)_i)^2 \rangle_{T_i}$ is the variance of the trap position during the measurement i . The second derivative of g can be expressed in terms of the variance, σ_i^2 , of the bead position in a fixed trap potential centered at $(\bar{z}_0)_i$. Straightforward calculation gives

$$\begin{aligned} \frac{\partial^2 g(z, z_0)}{\partial z_0^2} \Big|_{(\bar{z}_0)_i} &= g(z, (\bar{z}_0)_i) \left(\frac{\kappa_t}{k_B T} \right)^2 \sigma_i^2 \\ &\times \left[\left(\frac{z - \langle z \rangle_{(\bar{z}_0)_i}}{\sigma_i} \right)^2 - 1 \right]. \end{aligned} \quad (20)$$

Here, $\langle z \rangle_{(\bar{z}_0)_i} \hat{=} \sum_z z p_i(z|\phi)$ is the average position of the bead in a trap fixed at center position $(\bar{z}_0)_i$, and $\sigma_i^2 \hat{=} \langle z^2 \rangle_{(\bar{z}_0)_i} - \langle z \rangle_{(\bar{z}_0)_i}^2$ is the variance of the position of the bead. Fluctuations in the positions of the trap during a measurement i can be neglected if $\tilde{p}_i(z|\phi) \approx p_i(z|\phi)$, i.e., if $|\partial^2 g(z, z_0)/\partial z_0^2| \sigma_{T_i}^2 \ll g(z, (\bar{z}_0)_i)$ for typical values of z . Since the z -dependent term in the last bracket of Eq. (20) is of order $\mathcal{O}(1)$, one obtains the condition

$$\sigma_{T_i}^2 \ll \left(\frac{k_B T}{\kappa_t \sigma_i} \right)^2. \quad (21)$$

As an upper estimate for σ_i^2 one may simply use the observed variance of histogram N_i . Since we always observe that σ_i increases with increasing distance from the surface, we can take the worst case by using the variance of the distribution measured at a distance where the surface potential effectively is zero, $\sigma_i^2 = k_B T/\kappa_t$. Here, we obtain the condition, $(\sigma_{T_i}/\sigma_i)^2 \ll 1$. In the video microscopy method, the

typical values for this ratio are of the order $\sim 10^{-2}$, thus ensuring the applicability of Eqs. (16) and (17). Though we have no direct estimate of σ_{T_i} in the quadrant photodiode method, we are quite confident that condition Eq. (21) is satisfied here as well, due to the similarities of the two experimental setups.

5.3. Effect of a finite shutter time

An important experimental assumption underlying the measurement of the positional distribution of the bead is that the shutter time is sufficiently small compared to the autocorrelation time of the fluctuations. The effect of a finite shutter time can be estimated by assuming that the effective potential is approximately harmonic, $V_{z_0}(z) + \phi(z) \approx (1/2)(\tilde{\kappa}_t/k_B T)(z - \bar{z})^2$, where $\tilde{\kappa}_t$ is the total trap stiffness and \bar{z} is the average bead position (we neglect a possible offset to the potential which plays no role for the following discussion). Diffusion in a harmonic potential is described by the Einstein–Ornstein–Uhlenbeck theory, yielding the autocorrelation time, $\tau = k_B T/\tilde{\kappa}_t D$, where D is the diffusion constant [24]. For this process, the average position, $\langle z(z_0) \rangle_{\Delta t}$, of a bead initially located at z_0 and measured over a time window of Δt , is [29]

$$\langle z(z_0) \rangle_{\Delta t} = \bar{z} + (z_0 - \bar{z}) \exp(-\Delta t/\tau).$$

Consequently, the probability $p_{\Delta t}(z)$ for observing the average position z in a measurement with the shutter time Δt , reads

$$\begin{aligned} p_{\Delta t}(z) &= p_0(z_0) \left(\frac{d\langle z(z_0) \rangle_{\Delta t}}{dz_0} \right)^{-1} \\ &= \frac{\exp(\Delta t/\tau)}{\sqrt{2\pi}\sigma_0} \exp\left(-\frac{(z - \bar{z})^2 \exp(2\Delta t/\tau)}{2\sigma_0^2} \right), \end{aligned} \quad (22)$$

where p_0 is the true probability distribution of the bead (assumed to be approximately Gaussian) and $\sigma_0 = \sqrt{k_B T/\tilde{\kappa}_t}$ is the standard deviation. The expression for $p_{\Delta t}$ shows that the measured histogram is also a Gaussian distribution with a reduced standard deviation,

$$\sigma_{\Delta t} = \sigma_0 \exp(-\Delta t/\tau). \quad (23)$$

Using the quadrant photodiode method the autocorrelation time, τ , is found to be approximately between 4 and 15 ms in the probing regime. The fact that the diffusion is significantly decreased (see Fig. 5) close to the interface where the effective trap stiffness increases ensures that τ even close to the interface is still within this interval. However, to stay somewhat away from the interface, in the analysis we only include data where the interactions are below $\sim 12 k_B T$. The shutter time, $\Delta t = 2$ ms, used in the video microscopy method is not negligible compared to τ . Therefore, we need to include the effect of the associated truncation of the measured distributions as written in Eq. (23) when finding the interaction potentials, $\phi(z)$. The measured variance is a convolution of the true fluctuations and the experimental noise

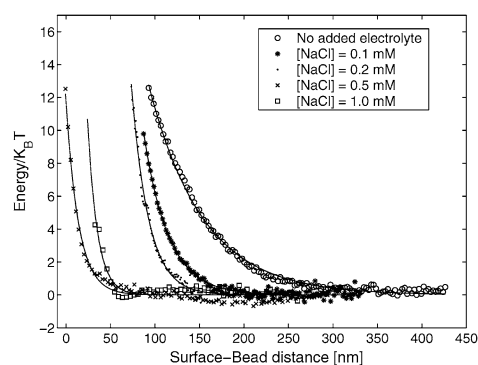


Fig. 8. Interaction potentials for a 0.97- μm silica bead and a glass coverslip at different electrolyte concentrations measured by the video microscopy method. The full lines are fits to the electrostatic term in Eq. (1) with ϕ_0 and κ as fitting parameters to the data.

σ_N which is extracted from a histogram of a bead stuck to the surface. Therefore, in order to account for this truncation, we use Eq. (23) and the assumption that the effective potential is approximately harmonic and multiply all the time series measured by the video method with the factor $\sigma_0/\sigma_{\Delta t}$, where σ_0 is found from Eq. (23) as $\sigma_0 = \sqrt{\sigma_{\Delta t}^2 - \sigma_N^2} \exp(\Delta t/\tau)$.

6. Interaction potentials

Using the methods described in the preceding sections we find interaction potentials between polystyrene or silica beads and glass surfaces at different electrolyte concentrations. Fig. 8 shows the interaction potentials between a 0.97- μm silica bead and a glass surface at [NaCl] concentrations of ≈ 0 –0.5 mM. At all concentrations the data fit nicely to the electrostatic term of the DLVO theory, Eq. (1); the fits are shown as full lines in Fig. 8. The van der Waals attractions are too weak to be visible in the interaction potential. The values obtained for the Debye lengths κ^{-1} are shown in Table 1 and are in good agreement with predictions of Eq. (4).

In pure water the ionization of the water itself gives $\kappa^{-1} \approx 960$ nm. The interaction potentials measured for both the silica and the polystyrene beads at [NaCl] ≈ 0 mM are consistent with Debye lengths substantially smaller than 960 nm which indicates the presence ($\sim 10^{-5}$ M) of ions from impurities in the suspension, a pollution which in practice is difficult to avoid. This presence of $\sim 10^{-5}$ M electrolytes might be due to the outgassing of sodium ions from

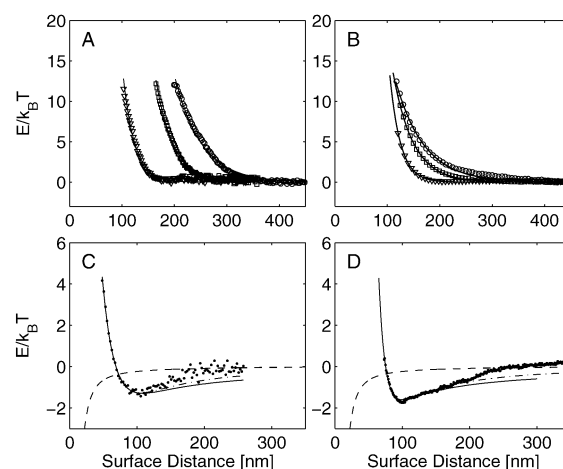


Fig. 9. Measured surface potentials for a 1.07- μm polystyrene bead and a glass coverslip at different electrolyte concentrations. The full lines in (A) and (B) show fits of the electrostatic part of Eq. (1) with ϕ_0 and κ as fitting parameters to the data. Symbols: \circ , 0 M; \square , 0.1 mM; ∇ , 0.2 mM; and \bullet , 0.5 mM. (A + C) Video microscopy method. (B + D) Quadrant photodiode method. The dashed lines in (C) and (D) show the Lifshitz theory. The dash-dotted lines in (C) and (D) are fits of Eq. (1) using the surface element integration, U_{SEI} , for the attractive part with ϕ_0 , κ , and A as fitting parameters. The full lines in (C) and (D) are also fits of Eq. (1) to data but using the Derjaguin's approximation, U_D , for the attractive part.

the coverglass; however, the concentration of ions does not appear to increase with time.

Fig. 9 shows the interaction potentials between a 1.07- μm polystyrene bead and a glass surface at [NaCl] ≈ 0 –0.5 mM. Fits of DLVO theory, Eq. (1), to data are shown as full lines in Fig. 9 and representative values obtained for the Debye lengths κ^{-1} are listed in Table 1. In the case of 0.1 and 0.2 mM electrolyte concentrations we cannot say if the discrepancy between the experimentally obtained Debye lengths and the predictions from DLVO theory arises from experimental uncertainties or because the theory is insufficient. However, as the Debye lengths deviate only a few nanometers from the result predicted by the theory, the interaction between the polystyrene beads and the glass surface at [NaCl] ≈ 0 –0.2 mM seems to be well described by DLVO theory.

DLVO theory predicts the existence of a secondary minimum in the potential energy where the attractive van der Waals force is balanced by the electrostatic repulsion. However, at electrolyte concentrations up to 0.2 mM, this minimum cannot be resolved by our methods. Only in measurements with polystyrene beads and electrolyte concen-

Table 1
Comparison of the Debye length, κ^{-1} experimentally obtained by the two different methods to the values predicted by DLVO theory

Electrolyte (NaCl) concentration	≈ 0 M	0.1 mM	0.2 mM	0.5 mM	1.0 mM
Polystyrene (video microscopy)	51 nm	32 nm	22 nm	18 nm	
Polystyrene (quadrant photodiode)	55 nm	43 nm	26 nm	11 nm	
Silica (video microscopy)	61 nm	28 nm	19 nm	14 nm	11 nm
DLVO predictions	960 nm	30.4 nm	21.5 nm	13.6 nm	9.6 nm

The polystyrene leads stuck to the surface at concentrations larger than 0.5 mM.

trations of 0.5 mM and larger the minimum in potential energy was resolved. At electrolyte concentrations of 0.5 mM there consistently and reproducibly is a transition in the potential energy landscape: For experiments which all, within experimental errors, had similar sizes of beads and $[\text{NaCl}] = 0.5 \text{ mM}$ the interaction potentials look rather different; some display a minimum and others do not. Typical interaction potentials at this concentration are shown in Figs. 9C (video method) and 9D (quadrant photodiode method). In these figures, minima in the interaction potentials due to the van der Waals attraction between the probe and the surface are evident at $\approx 100 \text{ nm}$ from the surface. The depth of these minima are $1.0\text{--}1.5 k_B T$.

Also, the energy landscape appears to change rapidly with respect to salt concentration; if the concentration of NaCl was slightly higher than 0.5 mM, the trapped beads would escape and jump to the glass surface before the measurement could be completed, consistent with the findings of [30]. In some rare cases we were able to perform measurements with $[\text{NaCl}] = 0.7 \text{ mM}$, these results being qualitatively similar to the measurements shown in Figs. 9C and 9D. For a silica–glass system the charge on silica surfaces is known to depend strongly on electrolyte concentration and pH [31]; something similar could be true for a polystyrene–glass system.

In Figs. 9C and 9D the measured interaction potentials at 0.5 mM NaCl are compared to existing theories. The full lines show least-square fits to the data of Eq. (1), with the attractive part U substituted by the Derjaguin's approximation U_D . The dash-dotted lines show fits of Eq. (1) using the surface element integration method, U_{SEI} , as the attractive part of the potential. In both cases, the Hamaker constant, κ , and ϕ_0 are used as fitting parameters and values obtained for κ^{-1} using the SEI method are given in Table 1. Only data points for distances smaller than 100 nm are included in the fit. Using U_{SEI} for the attractive part in Eq. (1) gives a better fit to the data than using U_D . In fact, Eq. (3) has been applied before with success to a similar system, but with $10 \mu\text{m}$ particles [32]. From the fit using U_{SEI} , the Hamaker constant is found to be $1.4 \times 10^{-20} \text{ J}$ for the video method and $1.5 \times 10^{-20} \text{ J}$ for the quadrant photodiode method, which compares very well to the value of $1.4 \times 10^{-20} \text{ J}$ given in Ref. [15] for the Hamaker constant for polystyrene beads in water without added electrolytes. Despite the agreement between the experiment and theory for the Hamaker constant and Debye lengths there is a qualitative difference between the data and the fitted curves and, in fact, this difference becomes more pronounced if the fits are extended out to $z \sim 300 \text{ nm}$. In particular, DLVO theory predicts a larger range of van der Waals attraction than observed. If the zero energy is not held fixed at zero for infinite separations, but is allowed to vary as a fitting parameter, then the fitting routine gives a result which qualitatively shows the same, namely that we observe a more short-range attraction than predicted by DLVO theory. Also, allowing the zero energy to vary causes it to take unphysical values of several $k_B T$ away from

zero far away from the surface where the interaction energy should be zero. Therefore, we have chosen to keep the zero energy fixed.

The dashed line in Figs. 9C and 9D is the full Lifshitz theory (Eq. (6)) which includes screening and retardation effects. Lifshitz theory makes the attraction fall off too fast in comparison to our measurements.

In the experiments with silica beads we do not see the minimum in the interaction potentials, even at high electrolyte concentrations. The zeta potential of silica beads has been measured to be higher than that of the polystyrene beads [33]. Therefore, the surface potential is higher and the electrostatic repulsion increased as seen from the prefactor in Eq. (1) and the minimum is not observed at these electrolyte concentrations.

Qualitative discrepancies between theory and experiments have been documented for polystyrene–surface interactions in the literature. For example, in [20] where larger polystyrene beads were used ($6 \mu\text{m}$) the attraction was found to fall off faster than predicted by Lifshitz theory. This is in contrast to our measurements where the interaction falls off slower than predicted by Lifshitz. In [30], at an electrolyte concentration around 0.5 mM, a discrepancy from DLVO was found for particles larger than in our measurements and it was proposed that the discrepancy could be due to the bead attaching to the surface through a single polystyrene polymer.

7. Summary

We have presented a novel method to determine the axial position of a bead with respect to the focus plane of a microscope objective based on its apparent diffraction pattern. The most important difference between our method and those described in literature is that we use the same bead for probing and calibration purposes which significantly improves the resolution in the direction parallel to the optical light path, which we find to be approximately 5 nm. This method is especially robust with respect to drift of the sample and can be used at any sizes of colloids placed anywhere within a sample. We used this method along with an optical trap to probe the interactions between glass surfaces and beads of polystyrene or silica in different electrolyte concentrations. The results were checked by an independent experimental method based on a quadrant photodiode detection scheme. Applying a novel maximum-likelihood method we obtain very detailed information about the underlying interaction potential. Our findings are consistent with DLVO theory for low salt concentrations. However, for high electrolyte concentrations, a qualitatively different behavior is seen which is not explained by any existing theories. The methods presented are also ideal for determining interactions between biological specimen such as bacteria or yeast cells and surfaces.

Acknowledgments

We thank Kirstine Berg-Sørensen for fruitful discussions and a careful reading of the manuscript. We are grateful for financial support from the NKT academy, the Danish research councils, the Carlsberg Foundation, Lundbeck, Foundation, and the BIOP graduate school.

References

- [1] A.C. Dogariu, Rajagopalan, *Langmuir* 16 (2000) 2770.
- [2] D. Grier, *Nature* 424 (2003) 810.
- [3] J. Gelles, B.J. Schnapp, M.P. Sheetz, *Nature* 331 (1988) 450.
- [4] F. Gittes, C.F. Schmidt, *Methods Cell Biol.* 55 (1998) 129.
- [5] J.C. Crocker, D.G. Grier, *J. Colloid Interface Sci.* 179 (1996) 298.
- [6] A.R. Clapp, R.B. Dickenson, *Langmuir* 17 (2001) 2182.
- [7] T. Ota, T. Sugiura, S. Kawata, *Appl. Phys. Lett.* 80 (2002) 3448.
- [8] J.M. Sharp, A.R. Clapp, R.B. Dickinson, *Colloids Surf. B* 27 (2003) 355.
- [9] A. Rohrbach, E.H.K. Stelzer, *Appl. Opt.* 41 (2002) 2494.
- [10] E. Fällman, O. Axner, *Appl. Opt.* 42 (2003) 3915.
- [11] D.C. Dennis, C. Prieve, *Adv. Colloid Interface Sci.* 82 (1999) 93.
- [12] C. Gosse, V. Croequette, *Biophys. J.* 82 (2002) 3314.
- [13] J.K. Dreyer, K. Berg-Sørensen, L. Oddershede, *Appl. Opt.* 43 (2004) 1991.
- [14] J. Ferkinghoff-Borg, *Eur. Phys. J. B* 29 (2002) 481.
- [15] J.N. Israelachvili, *Intermolecular and Surface Forces*, second ed., Academic Press, London, 1991.
- [16] B.A. Pailthorpe, W.B. Russel, *J. Colloid Interface Sci.* 89 (1982) 563.
- [17] S. Bhattacharjee, M. Elimelech, *J. Colloid Interface Sci.* 193 (1997) 273.
- [18] E.M. Lifshitz, *J. Exp. Theor. Phys.* 29 (1955) 94.
- [19] I.E. Dzyaloshinskii, E.M. Lifshitz, L.P. Pitaerskii, *Adv. Phys.* 10 (1961) 165.
- [20] M.A. Bevan, D.C. Prieve, *Langmuir* 15 (1999) 7925.
- [21] L.P. Ghislain, N.A. Switz, W.W. Webb, *Rev. Sci. Instrum.* 65 (1994) 2762.
- [22] A. Pralle, M. Prummer, E.-L. Florin, E.H.K. Stelzer, J.K.H. Hörber, *Microsc. Res. Techn.* 44 (1999) 378.
- [23] L. Oddershede, S. Grego, S.F. Nørrelykke, K. Berg-Sørensen, *Probe Microsc.* 2 (2001) 129.
- [24] K. Berg-Sørensen, H. Flyvbjerg, *Rev. Sci. Instrum.* 75 (2004) 594.
- [25] H. Brenner, *Chem. Eng. Sci.* 16 (1961) 242.
- [26] M.J. Lang, C.L. Asbury, J.W. Shaevitz, S.M. Block, *Biophys. J.* 83 (2002) 491.
- [27] A. Stuart, S.K. Old, *The Advanced Theory of Statistics*, vol. 1, sixth ed., Wiley, New York, 1994.
- [28] W.H. Press, et al., *Numerical Recipes in C*, second ed., Cambridge Univ. Press, 1992.
- [29] N.G. Van Kampen, *Stochastic Processes in Physics and Chemistry*, first ed., North-Holland/Elsevier Science, 1981.
- [30] S.H. Behrens, J. Plewa, D.G. Grier, *Eur. Phys. J. E* 10 (2003) 115.
- [31] S.H. Behrens, D.G. Grier, *J. Chem. Phys.* 115 (2001) 6716.
- [32] H.H. Grünberg, L. Helden, P. Leiderer, C. Bechinger, *J. Chem. Phys.* 114 (2001) 10094.
- [33] J.A. Brant, E. Childress, *J. Membr. Sci.* 203 (2002) 257.